

RESEARCH ARTICLE | OCTOBER 03 2023

## In search of a precursor for crystal nucleation of hard and charged colloids

Marjolein de Jager   ; Frank Smalenburg  ; Laura Filion 



*J. Chem. Phys.* 159, 134902 (2023)

<https://doi.org/10.1063/5.0161356>



CrossMark

## The Journal of Chemical Physics

### Special Topic: Algorithms and Software for Open Quantum System Dynamics

**Submit Today**

# In search of a precursor for crystal nucleation of hard and charged colloids

Cite as: J. Chem. Phys. 159, 134902 (2023); doi: 10.1063/5.0161356

Submitted: 9 June 2023 • Accepted: 13 September 2023 •

Published Online: 3 October 2023



Marjolein de Jager,<sup>1,a)</sup>  Frank Smalenburg,<sup>2</sup>  and Laura Filion<sup>1</sup> 

## AFFILIATIONS

<sup>1</sup>Soft Condensed Matter, Debye Institute of Nanomaterials Science, Utrecht University, Utrecht, The Netherlands

<sup>2</sup>Université Paris-Saclay, CNRS, Laboratoire de Physique des Solides, 91405 Orsay, France

<sup>a)</sup>Author to whom correspondence should be addressed: [m.e.dejager@uu.nl](mailto:m.e.dejager@uu.nl)

## ABSTRACT

The interplay between crystal nucleation and the structure of the metastable fluid has been a topic of significant debate over recent years. In particular, it has been suggested that even in simple model systems such as hard or charged colloids, crystal nucleation might be foreshadowed by significant fluctuations in local structure around the location where the nucleus first arises. We investigate this using computer simulations of spontaneous nucleation events in both hard and charged colloidal systems. To detect local structural variations, we use both standard and unsupervised machine learning methods capable of finding hidden structures in the metastable fluid phase. We track numerous nucleation events for the face-centered cubic and body-centered cubic crystals on a local level and demonstrate that all signs of crystallinity emerge simultaneously from the very start of the nucleation process. We thus conclude that we observe no precursor for the crystal nucleation of hard and charged colloids.

Published under an exclusive license by AIP Publishing. <https://doi.org/10.1063/5.0161356>

## I. INTRODUCTION

Crystal nucleation plays an important role in fields ranging from colloidal self-assembly, to protein crystallization, and even polymorph selection in pharmaceuticals.<sup>1,2</sup> However, despite its importance in a number of essential fields, the detailed mechanism of forming a crystal nucleus still remains a topic of continuous debate.

The simplest theory that addresses crystal nucleation is classical nucleation theory (CNT). In CNT, the metastable fluid is continuously undergoing thermal fluctuations, where small, solid clusters form and dissolve until one appears that is large enough (critically large) to grow out into a macroscopic crystal. The size of such a critical cluster is given simply by balancing the bulk free-energy gain associated with transitioning into the more stable solid phase, with the surface free-energy cost of having a finite crystal cluster immersed in the fluid. This picture, however, becomes significantly more complicated when one considers the possibility of multiple competing crystal structures, typically referred to as polymorphs. In systems with crystal polymorphs, the crystalline phase that first nucleates in the metastable fluid is not necessarily the stable phase. Theories to address such situations, such as the Ostwald step

rule,<sup>3</sup> and the Alexander–McTague theory<sup>4</sup> have proven unreliable in explaining polymorph selection (see, e.g., Refs. 5–7).

One complication when studying such questions is the close interplay between local structural motifs that occur naturally in the fluid and the ones that might emerge when the crystal forms. It has been suggested that motifs hiding in the fluid are predictive of, or even responsible for, the location or polymorph of the nucleus that forms.<sup>8,9</sup> To investigate this possibility, one avenue forward could be to explore just how much information the metastable liquid is hiding regarding the nucleation process. Over the last two decades, a plethora of studies have appeared presenting contradictory observations.<sup>8,10–19</sup> In particular, in simple systems such as charged colloids that nucleate into either the face-centered cubic (FCC) or body-centered cubic (BCC) crystal, some studies have argued that local structural order develops before the local density increases,<sup>8,15,16</sup> while other authors found evidence that the two processes happen simultaneously.<sup>17</sup>

To address this issue, some recent, intriguing studies have explored how modifying (via biasing) the structure of the fluid—either enhancing or suppressing specific local motifs—affects the nucleation process.<sup>6,15</sup> In principle, such studies might be able to give one direct evidence that a specific local structure either

enhances or suppresses the nucleation process. Unfortunately, however, biasing the structure of the fluid modifies not only its local structure but also its thermodynamics, meaning that comparisons with the unbiased case are inconclusive.

The more direct route to trying to explore how various kinds of local ordering interplay in crystal nucleation is simply to simulate the nucleation event and follow the various structural and density features as nucleation happens. At first glance, this would appear to be a straightforward approach. However, the challenge in this case lies in the difficulty of creating local order parameters that are unbiased. For example, order parameters that are tuned to distinguish the crystalline regions from the fluid might struggle at the boundary between the fluid and crystal—a highly important aspect at the beginning of nucleation. Similar issues exist for other order parameters, making it very difficult to pinpoint the start of the nucleation process and hence to determine whether structural order emerges before, during, or after densification. Hence, in some cases, instead of accurately capturing whether local structure exists in the highly fluctuating metastable fluid, one ends up examining the properties of the order parameter instead of those of the fluid.

While this problem is never fully avoidable, one option to try and avoid accidental biases is to exploit multiple different measures for local order. For instance, one can use measures associated with symmetries like bond-order parameters and order associated with the topological connections between neighboring particles—such as topological cluster classification (TCC). Interestingly, new unsupervised machine learning (UML) algorithms also give new avenues to probe structure (see, e.g., Refs. 20–29). Recent studies have even demonstrated that simple, UML-based approaches are able to extract variations in disorder in the structure of supercooled fluids from, e.g., a vector of bond order parameters.<sup>23,27,28</sup> Intriguingly, this includes identifying variations in local structure that are not easily extracted by looking at each element of the vector individually.

In this paper, we attempt to take the utmost care in identifying local signatures of the fluid and revisit the question: are there hidden local structures present in the metastable fluid that foreshadow the location of the imminent formation of a crystal nucleus? Specifically, we apply both classical and UML-based methods to the nucleation of hard and charged colloids in both the regimes of strong screening and weak screening, for which respectively the FCC and BCC crystals nucleate. To this end, we simulate numerous spontaneous nucleation events and closely follow all nucleation events as a function of time in search of a precursor. Note that throughout the literature, the definition of a precursor differs. Some studies define the initially formed structures, which are relatively more ordered than the fluid but are not yet fully crystalline, as precursor clusters. These initial structures, however, often already show both an increased structural ordering and an increased density. We define a precursor as regions that, prior to crystal nucleation, show a distinct delay between the increase in local density and local structural ordering, or the other way around. Similar to Ref. 17, we study the nucleation events by zooming in on the regions where the nuclei are born and analyzing the local fluctuations in density and structure of the metastable fluid. By doing this, we can locally track whether there is a delay between the increase in local structural ordering and local density, indicating the presence of a precursor. However, within the limits of this study, we find no evidence of such a precursor in the systems we studied.

**TABLE I.** For each system studied, the packing fraction of the supersaturated fluid  $\eta$  at which the brute force nucleation is performed together with the corresponding supersaturation  $\beta|\Delta\mu|$ . The last columns give the critical nucleus size  $n^*$  and barrier height  $\beta\Delta G^*$  obtained using umbrella sampling. The error in  $\beta\Delta G^*$  is no more than 1.

	$\beta\epsilon$	$1/\kappa\sigma$	$\eta$	$\beta \Delta\mu $	$n^*$	$\beta\Delta G^*$
FCC	Hard spheres		0.5385	0.585	75	16.5
	81	0.01	0.4681	0.584	84	16.3
	8	0.04	0.4400	0.541	69	14.8
BCC	81	0.40	0.1305	0.321	122	18.0

## II. MODEL

We consider a system of  $N$  like-charged hard spheres of diameter  $\sigma$  suspended in a solvent containing salt. The effective interaction potential between these colloids is given by the repulsive hard-core Yukawa potential

$$\beta\phi(r) = \begin{cases} \beta\epsilon \frac{e^{-\kappa\sigma(r/\sigma-1)}}{r/\sigma} & \text{for } r \geq \sigma, \\ \infty & \text{for } r < \sigma, \end{cases} \quad (1)$$

with contact value  $\beta\epsilon = Z^2\lambda_B/\sigma(1 + \kappa\sigma/2)^2$ , where  $Z$  is the charge of the colloids in electron charge,  $\lambda_B$  is the Bjerrum length,  $\kappa$  is the inverse Debye screening length, and  $\beta = 1/k_B T$ , with  $k_B$  being the Boltzmann constant and  $T$  being the temperature. Note that in the limit of zero charge ( $Z \rightarrow 0$ ) or infinite screening ( $\kappa\sigma \rightarrow \infty$ ), this potential reduces to the hard-sphere potential. The interaction potential was truncated and shifted such that the shift was never more than  $10^{-5}k_B T$ .

Nucleation of both the BCC and FCC phases in this system has been studied in the past (see, e.g., Refs. 30–34). In a previous study,<sup>34</sup> we used umbrella sampling to calculate the nucleation barriers and rates of highly screened charged particles. In this paper, we will study the nucleation of some of these (nearly-)hard systems as well as the nucleation of weakly screened charged particles. To be able to compare the nucleation processes of different systems, we select state points with approximately equal barrier heights. In particular, we will simulate brute-force nucleation events in systems with a barrier height of around  $15\text{--}18k_B T$ . Information on the nucleation barriers of the systems studied is given in Table I. Note that systems with a Debye screening length of  $1/\kappa\sigma = 0.01$  were found to behave essentially as “hard” spheres when mapped with an effective hard-sphere diameter.<sup>34</sup> A brief explanation of the methods used for computing the nucleation barriers as well as some additional information on these systems can be found in the supplementary material.

## III. METHODS

To explain the methods that we use for studying the nucleation events, we need to discuss two things: (i) how we identify local structure, and (ii) how we track nucleation events locally.

### A. Identifying local structure

We use three different methods to classify the local structure. The first method considers just the averaged bond-orientational order parameters (BOPs) of Lechner and Dellago.<sup>35</sup> For this, we first calculate the complex quantities for each particle  $i$

$$q_{lm}(i) = \frac{1}{N_b(i)} \sum_{j \in \mathcal{N}_b(i)} Y_l^m(\theta_{ij}, \phi_{ij}), \quad (2)$$

where  $\mathcal{N}_b(i)$  is the set of the  $N_b(i)$  nearest neighbors of particle  $i$ ,  $Y_{lm}(\theta, \phi)$  are the spherical harmonics with  $m \in [-l, l]$ , and  $\theta_{ij}$  and  $\phi_{ij}$  are the polar and azimuthal angles of the vector  $\mathbf{r}_{ij} = \mathbf{r}(j) - \mathbf{r}(i)$  connecting particles  $i$  and  $j$ . We use the SANN algorithm<sup>36</sup> to determine the nearest neighbors. Next, we average these complex quantities over the set of nearest neighbors as well as the particle itself

$$\bar{q}_{lm}(i) = \frac{1}{N_b(i) + 1} \sum_{j \in \{i, \mathcal{N}_b(i)\}} q_{lm}(j). \quad (3)$$

Finally, we compute the rotationally invariant averaged BOPs

$$\bar{q}_l(i) = \sqrt{\frac{4\pi}{2l+1} \sum_{m=-l}^l |\bar{q}_{lm}(i)|^2}, \quad (4)$$

and

$$\bar{w}_l(i) = \frac{w_l(i)}{(\sum_{m=-l}^l |\bar{q}_{lm}(i)|^2)^{3/2}}, \quad (5)$$

with

$$w_l(i) = \sum_{\substack{m_1, m_2, m_3 \\ m_1 + m_2 + m_3 = 0}} \begin{pmatrix} l & l & l \\ m_1 & m_2 & m_3 \end{pmatrix} q_{lm_1}(i) q_{lm_2}(i) q_{lm_3}(i), \quad (6)$$

where the term in brackets is the Wigner  $3j$  symbol, which is only non-zero when  $m_1 + m_2 + m_3 = 0$ . Note that  $w_l = 0$  when  $l$  is odd. Depending on the choice of  $l$ , these BOPs are sensitive to different (crystal) symmetries. For example,  $\bar{q}_6$  is very helpful in distinguishing more fluid-like environments from more solid-like environments such as FCC and BCC.<sup>35</sup>

While the BOPs are extremely useful for detecting specific symmetries in the local structure of the fluid, they are not necessarily optimal for detecting the most important structural variations in disordered systems, such as the metastable fluid. Recent work has shown that BOPs in combination with unsupervised machine learning algorithms are highly effective at autonomously detecting variations that might be difficult to see by studying the individual BOPs.<sup>22,23</sup> Hence, for the second method, we use an unsupervised algorithm to autonomously detect local structural fluctuations in the metastable fluid. In Ref. 22, Boattini *et al.* showed that a neural-network-based autoencoder, which is given  $\bar{q}_l$  with  $l \in [1, 8]$  as input, does a good job of distinguishing a whole range of different local structures. Similarly, in Ref. 25, van Damme *et al.* showed that using principal component analysis (PCA) as a dimensionality reduction method also does a good job of distinguishing the sizable assortment of crystal structures formed by rounded tetrahedra. For our system, we found that PCA and an autoencoder performed equally

well in distinguishing order and, hence, chose to use the simpler PCA algorithm in our analysis. To specifically focus on finding local fluctuations or signatures in the metastable fluid, we train the PCA model on  $\bar{q}_l$  with  $l \in [1, 8]$  of configurations containing only fluid particles and no (significant) solid nuclei. We then use this trained PCA model to analyze the entire nucleation trajectory. Note that in this way, the first principal component corresponds to the largest BOPs-related structural variation in the metastable fluid.

For the third and last method, we use an altogether different approach for classifying local structure. In particular, we use the topological cluster classification (TCC) algorithm developed by Malins *et al.*<sup>37</sup> to detect any local motifs that the BOPs might have overlooked. More specifically, we use TCC to calculate the population of certain types of clusters as well as the number of clusters of a certain type a particle is involved in.

Note that for computing the nucleation barriers, we additionally need a binary classification method that labels a particle as either fluid or solid. For this, we use the six-fold ten Wolde bonds<sup>38</sup>

$$d_6(i, j) = \frac{\sum_{m=-6}^6 q_{6m}(i) q_{6m}^*(j)}{\sqrt{(\sum_{m=-6}^6 |q_{6m}(i)|^2)(\sum_{m=-6}^6 |q_{6m}(j)|^2)}}, \quad (7)$$

where  $*$  indicates the complex conjugate and  $q_{6m}$  are the bond-orientational order parameters given by Eq. (2). Particle  $i$  is classified as solid if it has 6 or more neighboring particles  $j$  with which it has a solid-like bond, i.e.,  $d_6(i, j) > 0.7$ . We also use this fluid-solid classification to initially locate and follow the nucleation event. However, we want to point out that, although this provides a general overview of the nucleation event, it is not an ideal order parameter to study the onset of nucleation. Its binary nature with the thresholds for  $d_6(i, j)$  and the number of solid-like bonds causes it to overlook subtle increases in the local structural ordering of the fluid and hence reacts more slowly to the nucleation than other continuous order parameters.

### B. Simulating and tracking nucleation events

To obtain the spontaneous nucleation events, we use brute force Monte Carlo (MC), kinetic Monte Carlo (KMC), and molecular dynamics (MD) simulations in the NVT-ensemble, where we simulate  $N = 10\,976$  and  $N = 11\,664$  particles for the systems forming the FCC and BCC phases, respectively. The difference between the MC and KMC simulations is the acceptance ratio of the trial particle moves. For the MC simulations, this acceptance ratio is around 30%, whilst for the KMC simulations, it is around 85% resulting in dynamics that mimic Brownian motion.<sup>39</sup> The MD simulations are performed using LAMMPS with a Nose-Hoover thermostat.<sup>40</sup> We only perform MD simulations for the soft, hard-core Yukawa system, i.e., the one with  $1/\kappa\sigma = 0.40$ . As this system does not feel its hard core, it can simply be ignored. For each system studied, we analyze the order of ten nucleation events per simulation method. We do this by tracking the local density and structure to determine if there is a difference between the increase in local structural ordering and local density at the start of nucleation. To this end, for each nucleation event, we find the position  $\mathbf{r}_0$  that best captures the center of the nucleus at the start of nucleation. For this, we use the average center-of-mass of the precritical nucleus as a starting point and, if needed, adjust it by eye to best capture the birthplace of the



crystal nucleus. Next, for each snapshot of the nucleation trajectory, starting well before the start of nucleation, we determine all particles inside a sphere of radius  $R$  around  $\mathbf{r}_0$  and take the average of the local properties of these particles. This is similar to what Berryman *et al.* did in Ref. 17. The local structural properties that we consider are explained in Subsection III A. In addition, we define for each particle a local packing fraction measured via the volume of its Voronoi cell. The volumes of the Voronoi cells were obtained using voro++.<sup>41</sup> As we are searching for local precursors, we choose  $R$  such that the selected region contains around 30–40 particles. This size provides a good balance between being large enough to obtain relatively stable averages of the local properties and being small enough to ensure that the averaged properties still represent the local situation. Somewhat smaller or larger values for  $R$ , e.g., such that the region contains around 20 or 50 particles, do not significantly influence the trends we observe.

## IV. RESULTS

### A. Structure of the metastable fluid

Before we look into the actual crystal nucleation, we first characterize the structural properties of the metastable fluid. We start by examining the globally averaged values of the local BOPs. The results are shown in Fig. 1 for the metastable fluids of essentially hard spheres and of soft spheres as a function of the supersaturation. We see that  $\bar{q}_6$ ,  $\bar{q}_8$ , and  $\bar{w}_8$  are most prominent in both metastable fluids, and that all BOPs are only marginally affected by the increase in supersaturation. Furthermore, notice that the values in both systems are surprisingly similar, even though the metastable fluid of essentially hard spheres later forms an FCC crystal, whereas the fluid of the soft spheres will form a BCC crystal. The most prevalent difference between the two systems can be found in  $\bar{w}_6$ , which is smaller

for the essentially hard spheres than for the soft spheres, and for high supersaturation, it even becomes on average negative for the essentially hard spheres whereas it stays positive for the soft spheres. See the supplementary material for more analysis on the  $\bar{w}_i$ 's. Thus, we conclude that the fluid's "knowledge" about which crystal phase it should nucleate into is difficult to distinguish from the global values of the BOPs.

In addition to the BOPs, we take a look at the presence of the different TCC clusters in the metastable fluids. Figure 2 shows the population of various TCC clusters in the metastable fluid of hard spheres, nearly hard spheres, and soft spheres. The order of the most abundant clusters is very similar to the one observed by Taffs *et al.* in Ref. 42. As shown by Taffs *et al.*, the population is very sensitive to the packing fraction of the fluid; hence, any slight differences in the populations and their order most likely arise from a difference in supercooling.<sup>43</sup> Looking at Fig. 2, we observe that each cluster has

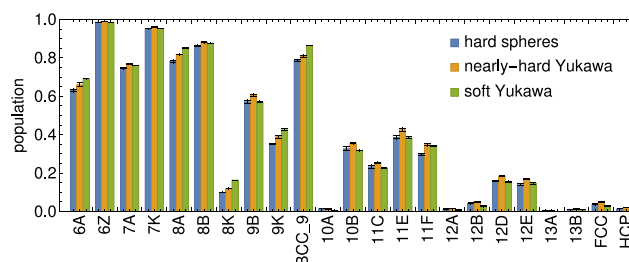


**FIG. 2.** The population of various TCC clusters in the metastable fluids of hard spheres ( $\eta = 0.5385$ ), nearly hard hard-core Yukawa particles ( $\beta\epsilon = 8$ ,  $1/\kappa\sigma = 0.04$ , and  $\eta = 0.4400$ ), and soft hard-core Yukawa particles ( $\beta\epsilon = 81$ ,  $1/\kappa\sigma = 0.40$ , and  $\eta = 0.1305$ ).

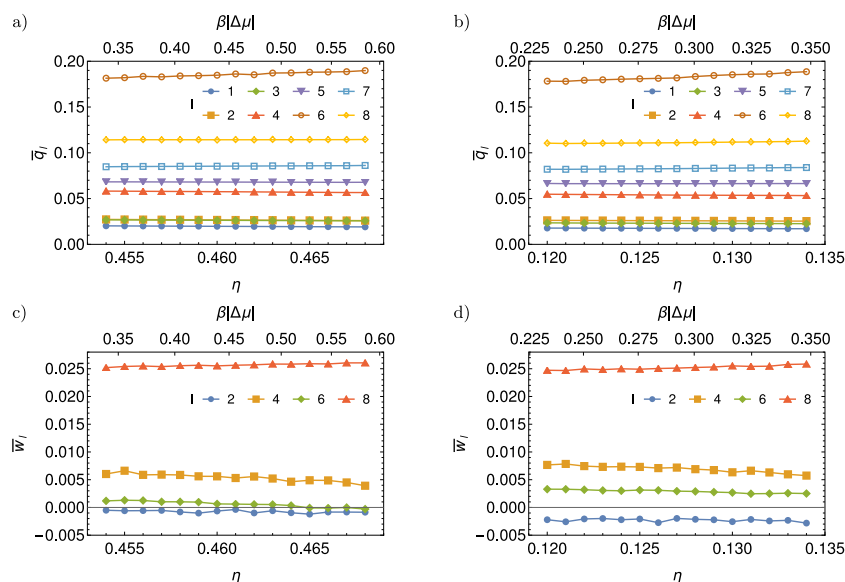


**FIG. 1.** The mean of (a), (b) the first eight  $\bar{q}_i$ 's and (c), (d) the first four even  $\bar{w}_i$ 's as a function of the supersaturation for the metastable fluids of hard-core Yukawa with (a), (c)  $\beta\epsilon = 81$  and  $1/\kappa\sigma = 0.01$ , and (b), (d)  $\beta\epsilon = 81$  and  $1/\kappa\sigma = 0.40$ .

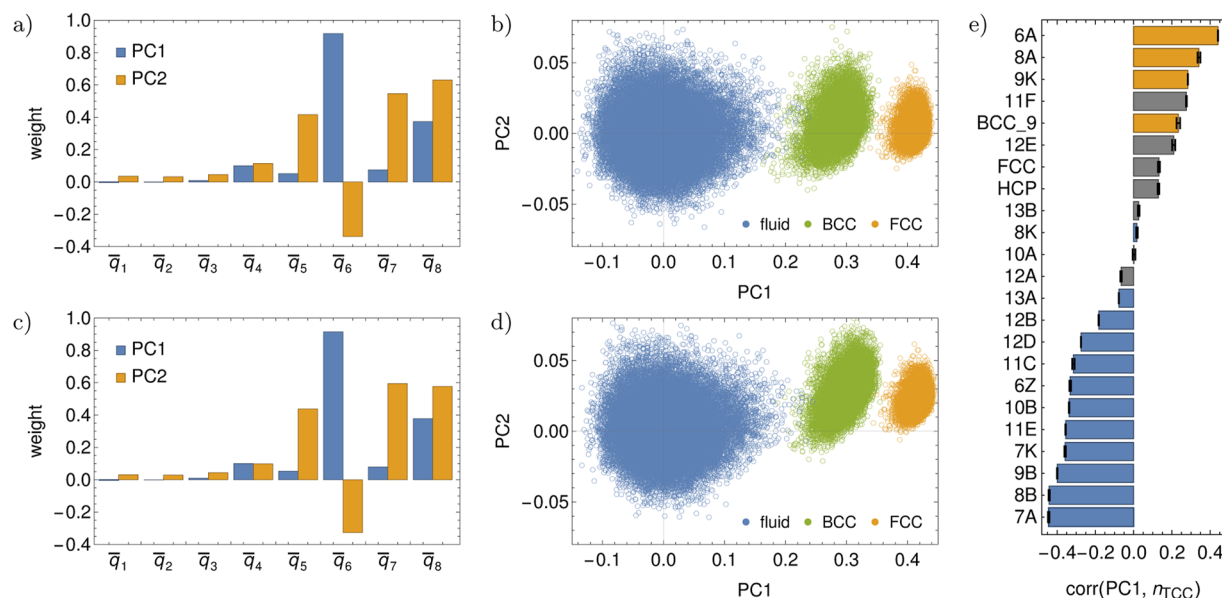


**FIG. 3.** PCA on the metastable fluids of (a), (b) hard spheres ( $\eta = 0.5385$ ) and (c), (d) soft hard-core Yukawa particles ( $\beta\epsilon = 81$ ,  $1/\kappa\sigma = 0.40$ , and  $\eta = 0.1305$ ). (a) and (c) Give the weight of each BOP in the first and second principal component. (b) and (d) Show the distribution of the fluid particles in the PC1–PC2 plane, with the addition of the corresponding bulk FCC phase of hard spheres ( $\eta = 0.5981$ ) and bulk BCC phase of soft hard-core Yukawa ( $\beta\epsilon = 81$ ,  $1/\kappa\sigma = 0.40$ , and  $\eta = 0.1311$ ). (e) Pearson correlation between PC1 and the number of TCC clusters a particle is involved in for the fluid of hard spheres. The color of the bars indicates clusters that consist of one or more tetrahedral subclusters (blue), one or more square pyramidal subclusters (yellow), or both/neither (gray).

a surprisingly similar population in all three metastable fluids. Any observed small deviations—such as the 6A, 8A, 8K, 9K, and BCC\_9 clusters, which have a slightly higher population in the fluid of soft spheres, and the 9B, 10B, 11C, 11E, and 12D clusters, which have a slightly higher population in the fluid of nearly hard spheres—can just as well be caused by a slight difference in supercooling between the three different metastable fluids. This indicates once more that it is difficult to determine which crystal phase will nucleate from the metastable fluid for the systems studied here.

Next, we characterize the local ordering of the metastable fluid on the single-particle level. As explained in the Methods, we train a PCA model using only configurations of the metastable fluid. In all cases, the first principal component (PC1) explains around 70% of the total variance of the input. To illustrate what kind of fluctuations PCA picks up in the fluid, Figs. 3(a) and 3(c) show for the metastable fluids of hard spheres and of soft spheres the weight of each BOP in the first and second principal components. We see that PC1 is mostly made up of  $\bar{q}_6$  and  $\bar{q}_8$ . Furthermore, Figs. 3(b) and 3(d) show

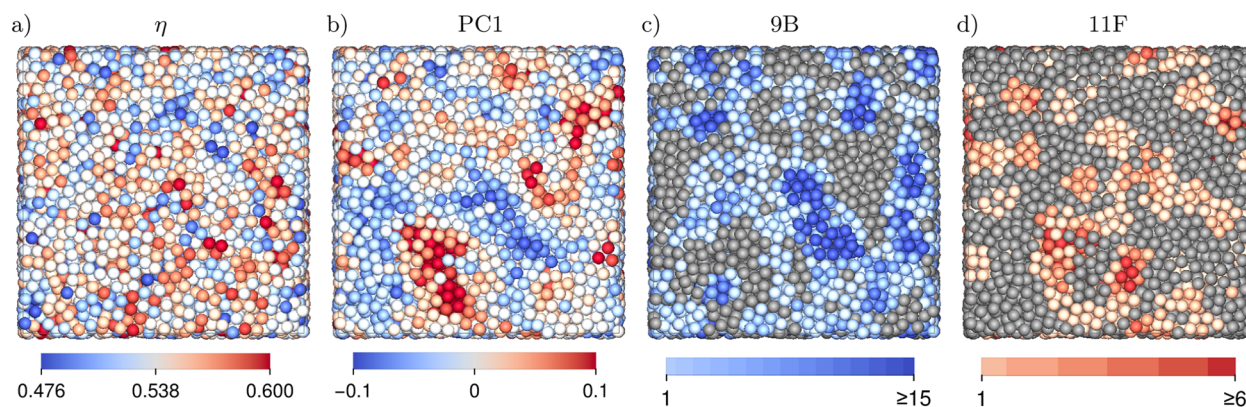


**FIG. 4.** A snapshot of the metastable fluid of hard spheres ( $\eta = 0.5385$ ) colored by (a) the local packing fraction, (b) the first principal component, (c) the number of 9B clusters per particle, and (d) the number of 11F clusters per particle.

the distribution of these metastable fluid particles in the PC1–PC2 plane, as well as the distributions of the corresponding FCC and BCC phases. (Recall that the data for the crystalline particles was not used in training the PCA models.) In this scatter plot, we can neatly see that the crystal phases lie in the region of large PC1. To get a better understanding of the real-space distribution of these particles with above or below average PC1, we take a look at a single snapshot of the metastable fluid of hard spheres and color the particles according to their local packing fraction, PC1, and the number of 9B and 11F clusters a particle is involved in, see Fig. 4. Even though the spatial correlations in the local packing fraction are not clearly visible, we can clearly distinguish by eye large spatial regions of above or below average PC1. The autocorrelation functions of these spatial correlations can be found in the supplementary material. Notice that the regions with above average PC1 correspond to an absence of 9B clusters and a high presence of 11F clusters, while regions with below average PC1 correspond to a high presence of 9B clusters and an absence of 11F clusters. Thus, there is a negative correlation between PC1 and 9B clusters and a positive correlation between PC1 and 11F. The precise correlations of these two and other TCC clusters with PC1 are shown in Fig. 3(e). Analogous to what was found in Ref. 23, the TCC clusters can be roughly divided into two groups: those with a negative correlation, which essentially are all clusters consisting of one or more tetrahedral subclusters,

and those with a positive correlation, which contain the clusters consisting of one or more square pyramidal subclusters.

Combining the observation of large spatial regions of above average PC1 with the proximity of these particles to the crystal phases in the PC1–PC2 scatter plot (Fig. 3), we can conclude that regions of above average PC1 form a good candidate for harboring a precursor for crystal nucleation. In Sec. IV B, we will investigate these regions while tracking the nucleation events. However, before we turn our attention to that, we need to determine the temporal correlations of the local structure so that we know the time window prior to the start of nucleation in which we can search for a precursor. Figure 5 shows, for multiple simulation methods, the autocorrelation functions (ACFs) of the first two principal components and the local packing fraction in the metastable fluids of hard spheres and of soft spheres. Here, we give the time in terms of the long-time diffusion time  $\tau_d = \sigma^2/6D_l$ , where  $D_l$  is the long-time diffusion coefficient obtained from the mean-squared displacement. Notice that the ACFs are essentially independent of the simulation method, which confirms that the dynamics are also independent of the choice of simulation method. We see in both systems that PC2 and the local packing fraction decay extremely fast over time. Although PC1 decays more slowly, i.e., within half a diffusion time for the hard spheres and one diffusion time for the soft spheres, this is still relatively fast. Other studies have shown similar results of fast

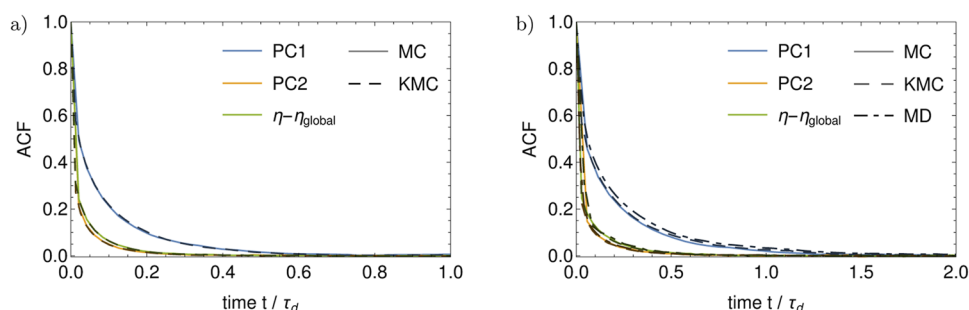


**FIG. 5.** Autocorrelation function of the first and second principal components and the local packing fraction in the metastable fluids of (a) hard spheres ( $\eta = 0.5385$ ) and (b) soft hard-core Yukawa particles ( $\beta\epsilon = 81$ ,  $1/\kappa\sigma = 0.40$ , and  $\eta = 0.1305$ ). The different dashed and darkness of the color indicate the simulation method, and the time is in terms of the long-time diffusion time  $\tau_d$ .

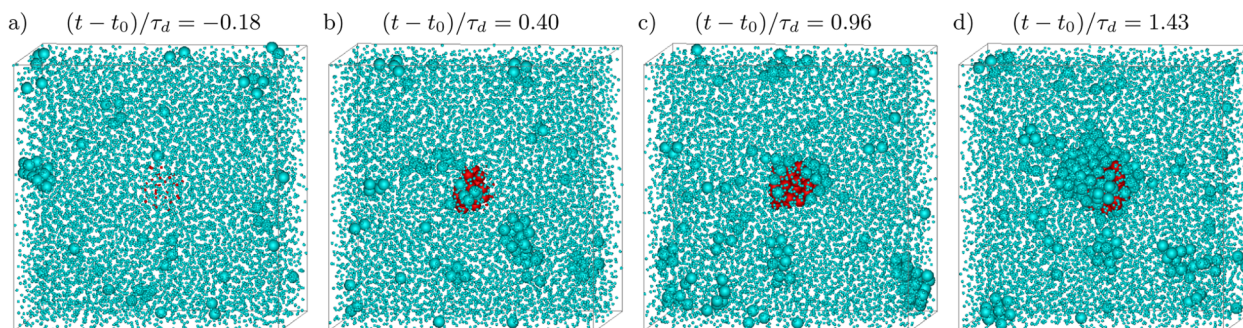


**FIG. 6.** (a)–(d) A snapshot of a typical nucleation event of hard spheres ( $\eta = 0.5385$ ) at four different times. Here  $t_0$  indicates the start of nucleation, and time is given in terms of the long-time diffusion time  $\tau_d$ . Fluid particles are displayed at a quarter of their actual size to make the nucleus visible, and red indicates the particles inside the studied region, i.e., those inside the sphere of radius  $R$  around the center of nucleation  $\mathbf{r}_0$ .



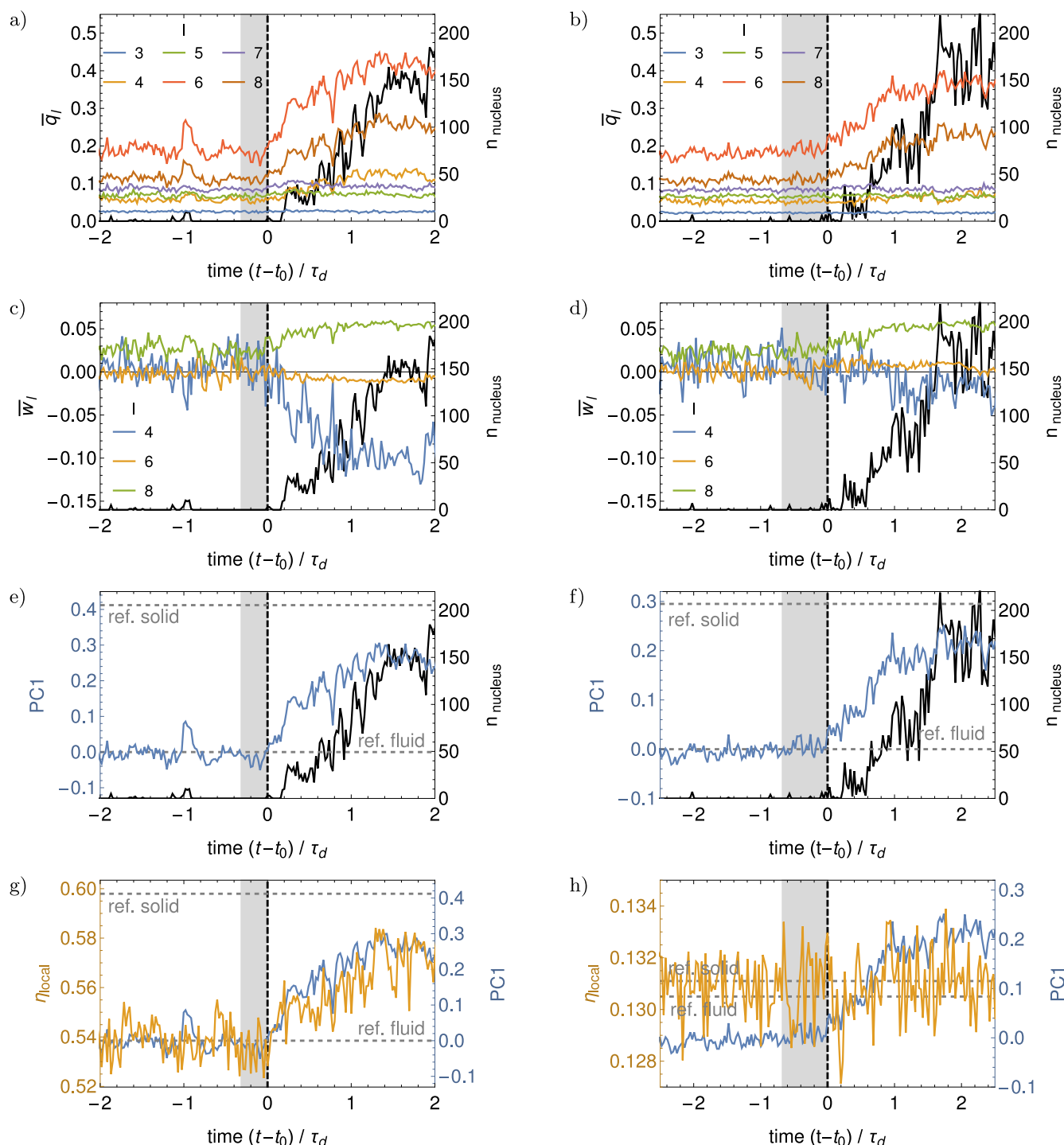


**FIG. 7.** Left: typical nucleation event of hard spheres ( $\eta = 0.5385$ ), same as in Fig. 6. Right: typical nucleation event of soft hard-core Yukawa particles ( $\beta\epsilon = 81$ ,  $1/\kappa\sigma = 0.40$ , and  $\eta = 0.1305$ ). Both events were obtained using MC simulations. The vertical dashed line in each figure indicates the start of nucleation  $t_0$ , and the shaded area indicates the time window before  $t_0$  for which the ACF of PC1  $> 0.05$  (see Fig. 5). In (a)–(f), the black line (right axis) gives the size of the biggest nucleus present in the studied region. The other lines give the average values of (a) and (b)  $\bar{q}_l$  for  $l \in [3, 8]$ , (c) and (d)  $\bar{w}_l$  for  $l \in [4, 6, \text{and } 8]$ , (e) and (f) PC1. In (g) and (h), the blue line (right axis) gives PC1, while the yellow line (left axis) gives the local packing fraction  $\eta_{\text{local}}$ . Note that in (e)–(g), the horizontal dashed lines give the reference value of PC1 in the fluid and solid phases. In (g), the right axis is scaled in such a way that the reference values in the fluid and solid of PC1 and  $\eta_{\text{local}}$  lie on top of each other. In (h), the horizontal dashed lines give the reference value of  $\eta_{\text{local}}$  in the fluid and solid phases.

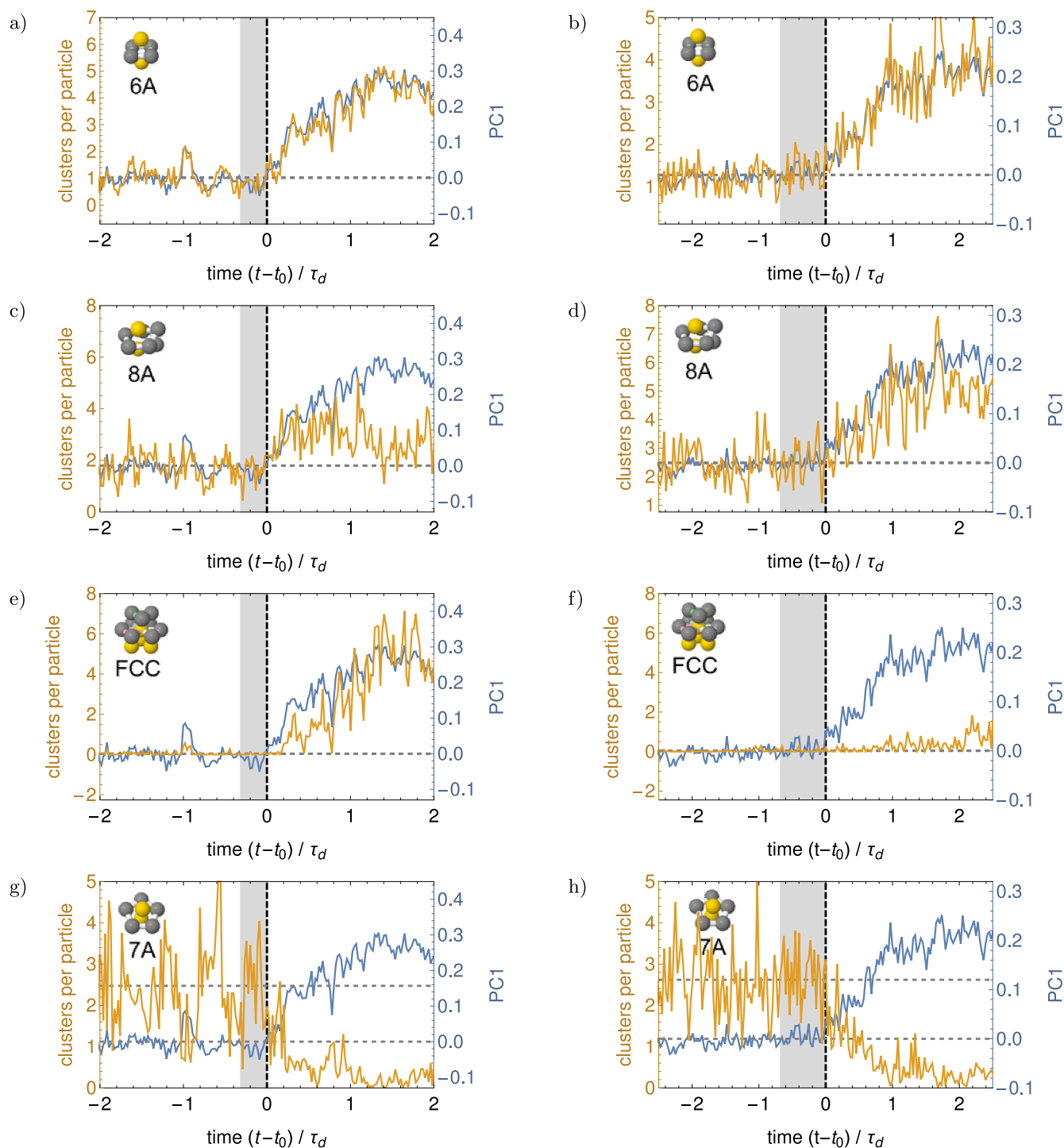


**FIG. 8.** For the same events as in Fig. 7, i.e., hard spheres (left) and soft hard-core Yukawa particles (right), the average number of clusters per particle (left axis, yellow) for a couple of TCC clusters together with the average value of PC1 (right axis, blue). The horizontal dashed lines indicate the reference values of the number of clusters per particle and PC1 in the fluid. In (a)–(f), the left axis is scaled in such a way that these lines lie on top of each other. In (g) and (h), this was not possible without inverting one of the axes.



decaying clusters of local ordering in (metastable) fluids.<sup>14,42</sup> In the supplementary material, we show the additional ACFs of the independent BOPs, which decay as fast as, or even faster than, PC1. The decay time of PC1 thus provides a good estimate for the time window prior to the start of nucleation in which we can search for a precursor.

## B. Nucleation study

We now turn our attention to crystal nucleation. As explained in the Methods, we simulate numerous spontaneous nucleation events using MC, KMC, and MD simulations, and track for all these events the local properties of the region where nucleation starts. Here, we discuss our observations using two typical nucleation events: one of the hard-spheres system and one of the soft spheres ( $\beta\epsilon = 81$  and  $1/\kappa\sigma = 0.40$ ). Both of these nucleation events were obtained using MC simulations. More nucleation events, where we either used other simulation methods or studied the other systems mentioned in Table I, can be found in the supplementary material. To better illustrate which region we study while tracking a nucleation event, Fig. 6 shows a couple of snapshots of the nucleation event of hard spheres, where the particles inside the studied region are colored red. For the same event, Fig. 7 shows the average properties of the particles in this studied region. In addition, Fig. 7 shows these same averaged properties for a nucleation event of soft spheres. Before we discuss what we see, let us again point out that the nucleus size (black line) is not an ideal order parameter for tracking the onset of crystal nucleation since its binary nature causes it to overlook subtle increases in the local structural ordering at the onset of nucleation. It does, however, provide a general overview of the nucleation event, such as when the nucleus reaches its critical size (see Table I). That being said, let us first discuss the BOPs of the studied region. We observe no notable change in the behavior of the BOPs before the start of nucleation, but, as soon as nucleation starts, we see a sharp increase in the values of  $\bar{q}_6$  and  $\bar{q}_8$  for both systems. Furthermore, for the hard spheres, we see that, once nucleation starts,  $\bar{q}_4$  increases,  $\bar{w}_6$  stays negative, and  $\bar{w}_4$  decreases. This all indicates that indeed the FCC phase nucleates. On the other hand, for the soft spheres, we see that, once nucleation starts,  $\bar{q}_4$  barely increases,  $\bar{w}_6$  stays positive, and  $\bar{w}_4$  keeps fluctuating around zero, which all indicates that indeed the BCC phase nucleates. Similar to the behavior of the BOPs, we observe no notable change in the behavior of PC1 before the start of nucleation, but see a sharp increase in its value once nucleation starts. Note that this increase in PC1 is visible before the number of particles classified as crystalline starts to rise (black line), demonstrating that PC1 is a better order parameter for tracking the start of nucleation than the nucleus size. Furthermore, note that PC1 has not yet reached the reference value of the bulk crystal by the end of the simulation. This is not unexpected, as the still relatively small nuclei cannot be regarded as consisting of a bulk crystal phase. Considerably larger nucleus sizes are needed for that. Lastly, for the hard spheres, we see that the local packing fraction increases simultaneously with PC1 as soon as nucleation starts. Moreover, no notable change in behavior can be observed before the start of nucleation. This strongly indicates that an increase in structural ordering and local density go together and, thus, that there is no apparent precursor. Unfortunately, as the difference between the packing fraction of the fluid and solid phases is extremely small for

the soft spheres, i.e., less than 0.001, it is not possible to observe any increase in the local packing fraction on top of the normal fluctuations. Hence, we cannot draw any conclusions on the local packing fraction of the soft spheres.

Next, to show that we have not missed any subtle changes in the local structure and thus to confirm that there is no precursor for nucleation, we further examine the local structure using TCC. In Fig. 8, we show for four of the most relevant TCC clusters the average number of clusters a particle is involved in and compare it with PC1. These four clusters are: (i) 6A, which has the strongest positive correlation with PC1 and is present in both bulk FCC and bulk BCC, (ii) 8A, which has the second strongest positive correlation with PC1 and is present in bulk BCC but not bulk FCC, (iii) FCC, which is present in bulk FCC but not bulk BCC, and (iv) 7A, which has the strongest negative correlation with PC1 and can neither be found in bulk FCC nor bulk BCC. Similar figures for other TCC clusters can be found in the supplementary material. For all clusters, we see that there is no significant change prior to the start of nucleation. Furthermore, we see that the trends of the 6A cluster coincide almost perfectly with those of PC1. Similarly, we see that the trends of the 8A cluster closely follow the trends of PC1. However, for hard spheres, the initial increase in 8A clusters is followed by a decrease. Since 8A is a cluster that is usually found in bulk BCC and not in bulk FCC, this initial increase might be surprising. It can, however, be explained via the observation that 8A clusters are found in high concentrations near the surface of growing nuclei.<sup>9</sup> As a result, the number of these clusters decreases once the nucleus grows beyond our averaging radius. For the FCC cluster, we observe a sharp increase during the nucleation of hard spheres. Notice, however, that this increase starts slightly later than the increase in PC1. This is not surprising as the FCC cluster is a relatively large cluster, i.e., it contains 13 particles, and consequently is not present in the first stages of nucleation. For the soft spheres, there is no significant increase in FCC clusters, as expected. Lastly, we take a look at the 7A cluster. In contrast to the other three clusters, this five-fold symmetric cluster has a strong negative correlation with PC1. Moreover, it is strongly present in the metastable fluid phases, whereas its presence in the FCC and BCC phases is negligible. It is, therefore, not surprising that we observe an immediate and sharp decrease in 7A clusters as soon as nucleation starts.

## V. CONCLUSIONS

To conclude, we have characterized the local structure of various metastable fluids of charged colloids using multiple methods: bond-orientational order parameters (BOPs), principal component analysis (PCA) on the BOPs, and topological cluster classification (TCC). In doing this, we have attempted to avoid artifacts due to biases in our chosen order parameters. For all systems, we have found that any local structural ordering has a relatively short lifetime, resulting in a short time window prior to the start of nucleation in which a precursor could exist. By tracking the local structure of the spatial region coinciding with the birthplace of the crystal nucleus, we show that inside this time window, no atypical behavior in the local structural order is observed using any of our structural order parameters. Furthermore, we demonstrate that all structural characteristics that differ significantly between the fluid and crystal phases start changing simultaneously as soon as nucleation starts.

Specifically, in the case of FCC, this includes the local density, which starts growing immediately as soon as structural order emerges. Thus, we conclude that we find no evidence for a precursor for the crystal nucleation of hard and charged colloids.

## SUPPLEMENTARY MATERIAL

In the supplementary material, we provide additional information on the nucleation barriers and the methods used for obtaining them, as well as additional analysis on structural correlations in the metastable fluids. Furthermore, the supplementary material contains the tracking results of additional nucleation events.

## ACKNOWLEDGMENTS

L.F. and M.d.J. acknowledge funding from the Vidi research program with Project No. VI.VIDI.192.102, which is financed by the Dutch Research Council (NWO).

## AUTHOR DECLARATIONS

### Conflict of Interest

The authors have no conflicts to disclose.

## Author Contributions

**Marjolein de Jager:** Conceptualization (supporting); Formal analysis (lead); Methodology (lead); Software (lead); Visualization (lead); Writing – original draft (lead); Writing – review & editing (equal). **Frank Smellenburg:** Conceptualization (supporting); Writing – review & editing (equal). **Laura Filion:** Conceptualization (lead); Funding acquisition (lead); Supervision (lead); Writing – original draft (supporting); Writing – review & editing (equal).

## DATA AVAILABILITY

The data that support the findings of this study are openly available in Zenodo at <https://doi.org/10.5281/zenodo.8337501>.<sup>44</sup>

## REFERENCES

- <sup>1</sup>S. Karthika, T. Radhakrishnan, and P. Kalaichelvi, *Cryst. Growth Des.* **16**, 6663 (2016).
- <sup>2</sup>G. C. Sosso, J. Chen, S. J. Cox, M. Fitzner, P. Pedevilla, A. Zen, and A. Michaelides, *Chem. Rev.* **116**, 7078 (2016).
- <sup>3</sup>W. Ostwald, *Z. Phys. Chem.* **22U**, 289 (1897).
- <sup>4</sup>S. Alexander and J. McTague, *Phys. Rev. Lett.* **41**, 702 (1978).
- <sup>5</sup>J. Russo and H. Tanaka, *Soft Matter* **8**, 4206 (2012).
- <sup>6</sup>J. Taffs and C. Patrick Royall, *Nat. Commun.* **7**, 13225 (2016).

- <sup>7</sup>W. Ouyang, C. Fu, Z. Sun, and S. Xu, *Phys. Rev. E* **94**, 042805 (2016).
- <sup>8</sup>J. Russo and H. Tanaka, *Sci. Rep.* **2**, 505 (2012).
- <sup>9</sup>W. Gispen, G. M. Coli, R. van Damme, C. P. Royall, and M. Dijkstra, *ACS Nano* **17**, 8807–8814 (2023).
- <sup>10</sup>P. R. ten Wolde and D. Frenkel, *Phys. Chem. Chem. Phys.* **1**, 2191 (1999).
- <sup>11</sup>T. Schilling, H. J. Schöpe, M. Oettel, G. Opletal, and I. Snook, *Phys. Rev. Lett.* **105**, 025701 (2010).
- <sup>12</sup>J. Russo and H. Tanaka, *J. Chem. Phys.* **145**, 211801 (2016).
- <sup>13</sup>P. Tan, N. Xu, and L. Xu, *Nat. Phys.* **10**, 73 (2014).
- <sup>14</sup>M. Li, Y. Chen, H. Tanaka, and P. Tan, *Sci. Adv.* **6**, eaaw8938 (2020).
- <sup>15</sup>Y.-C. Hu and H. Tanaka, *Nat. Commun.* **13**, 4519 (2022).
- <sup>16</sup>Y. Lu, X. Lu, Z. Qin, and J. Shen, *Solid State Commun.* **217**, 13 (2015).
- <sup>17</sup>J. T. Berryman, M. Anwar, S. Dorosz, and T. Schilling, *J. Chem. Phys.* **145**, 211901 (2016).
- <sup>18</sup>H. Tanaka, H. Tong, R. Shi, and J. Russo, *Nat. Rev. Phys.* **1**, 333 (2019).
- <sup>19</sup>W. Lechner, C. Dellago, and P. G. Bolhuis, *Phys. Rev. Lett.* **106**, 085701 (2011).
- <sup>20</sup>S. Becker, E. Devijver, R. Molinier, and N. Jakse, *Phys. Rev. E* **105**, 045304 (2022).
- <sup>21</sup>W. F. Reinhart, A. W. Long, M. P. Howard, A. L. Ferguson, and A. Z. Panagiotopoulos, *Soft Matter* **13**, 4733 (2017).
- <sup>22</sup>E. Boattini, M. Dijkstra, and L. Filion, *J. Chem. Phys.* **151**, 154901 (2019).
- <sup>23</sup>E. Boattini, S. Marín-Aguilar, S. Mitra, G. Foffi, F. Smellenburg, and L. Filion, *Nat. Commun.* **11**, 5479 (2020).
- <sup>24</sup>G. M. Coli and M. Dijkstra, *ACS Nano* **15**, 4335 (2021).
- <sup>25</sup>R. van Damme, G. M. Coli, R. van Roij, and M. Dijkstra, *ACS Nano* **14**, 15144 (2020).
- <sup>26</sup>A. Gardin, C. Perego, G. Doni, and G. M. Pavan, *arXiv:2112.08044* (2021).
- <sup>27</sup>D. Coslovich, R. L. Jack, and J. Paret, *J. Chem. Phys.* **157**, 204503 (2022).
- <sup>28</sup>J. Paret, R. L. Jack, and D. Coslovich, *J. Chem. Phys.* **152**, 144502 (2020).
- <sup>29</sup>C. S. Adorf, T. C. Moore, Y. J. Melle, and S. C. Glotzer, *J. Phys. Chem. B* **124**, 69 (2019).
- <sup>30</sup>S. Auer and D. Frenkel, in *Advanced Computer Simulation*, Advances in Polymer Science Vol. 173 (Springer, 2005), pp. 149–208 (2005).
- <sup>31</sup>C. Desgranges and J. Delhommelle, *J. Chem. Phys.* **126**, 054501 (2007).
- <sup>32</sup>A. R. Browning, M. F. Doherty, and G. H. Fredrickson, *Phys. Rev. E* **77**, 041604 (2008).
- <sup>33</sup>W. Gispen and M. Dijkstra, *Phys. Rev. Lett.* **129**, 098002 (2022).
- <sup>34</sup>M. de Jager and L. Filion, *J. Chem. Phys.* **157**, 154905 (2022).
- <sup>35</sup>W. Lechner and C. Dellago, *J. Chem. Phys.* **129**, 114707 (2008).
- <sup>36</sup>J. A. van Meel, L. Filion, C. Valeriani, and D. Frenkel, *J. Chem. Phys.* **136**, 234107 (2012).
- <sup>37</sup>A. Malins, S. R. Williams, J. Eggers, and C. P. Royall, *J. Chem. Phys.* **139**, 234506 (2013).
- <sup>38</sup>P. R. ten Wolde, M. J. Ruiz-Montero, and D. Frenkel, *Faraday Discuss.* **104**, 93 (1996).
- <sup>39</sup>E. Sanz and D. Marenduzzo, *J. Chem. Phys.* **132**, 194102 (2010).
- <sup>40</sup>S. Plimpton, *J. Comput. Phys.* **117**, 1 (1995).
- <sup>41</sup>C. Rycroft, *Chaos* **19**, 041111 (2009).
- <sup>42</sup>J. Taffs, S. R. Williams, H. Tanaka, and C. P. Royall, *Soft Matter* **9**, 297 (2013).
- <sup>43</sup>Note that any other differences with Ref. 42 stem from the fact that we consider more TCC clusters than Ref. 42 and that the populations in Ref. 42 are adapted such that particles which are members of more than one cluster are taken to reside only in the largest cluster.
- <sup>44</sup>M. de Jager, F. Smellenburg, and L. Filion (2023). “In search of a precursor for crystal nucleation of hard and charged colloids,” Zenodo, Dataset, <https://doi.org/10.5281/zenodo.8337501>.